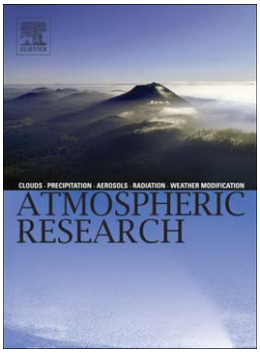

The influence of topography on vertical velocity of air in relation to severe storms near the Southern Andes Mountains

A. de la Torre, H. Pessano, R. Hierro, R. Santos, P. Llamedo, P. Alexander

PII: S0169-8095(15)00009-5
DOI: doi: 10.1016/j.atmosres.2014.12.020
Reference: ATMOS 3326

To appear in: *Atmospheric Research*

Received date: 27 August 2014
Revised date: 24 December 2014
Accepted date: 30 December 2014

Please cite this article as: de la Torre, A., Pessano, H., Hierro, R., Santos, R., Llamedo, P., Alexander, P., The influence of topography on vertical velocity of air in relation to severe storms near the Southern Andes Mountains, *Atmospheric Research* (2015), doi: 10.1016/j.atmosres.2014.12.020

The influence of topography on vertical velocity of air in relation to severe storms near the Southern Andes Mountains

A. de la Torre[a], H. Pessano[b,c], R. Hierro[a], R. Santos[c,e], P. Llamedo[a], P. Alexander[d]

[a]Facultad de Ingeniería, Universidad Austral, Avda. J. de Garay 125, C1063ABB Buenos Aires, Argentina

[b] Facultad Regional San Rafael, Universidad Tecnológica Nacional, Avda. Urquiza 314, M5602GCH San Rafael, Mendoza, Argentina

[c] Dirección de Agricultura y Contingencias Climáticas, Gobierno de Mendoza, San Martín 1850, M5560EWS Mendoza, Argentina

[d] Departamento de Física, FCEN, Universidad de Buenos Aires, Ciudad Universitaria, C1428EGA Buenos Aires, Argentina

[e] Instituto de Ciencias Básicas, Facultad de Ciencias Exactas y Naturales, Universidad de Cuyo, CPM5502JMA, Mendoza, Argentina

Corresponding author: A. de la Torre, Facultad de Ingeniería, Universidad Austral, Mariano Acosta 1901, 1629 Pilar, Buenos Aires, Argentina (adelatorre@austral.edu.ar).

Abstract

On the basis of 180 storms which took place between 2004 and 2011 over the province of Mendoza (Argentina) near to the Andes Range at southern mid-latitudes, we consider those registered in the northern and central crop areas (oases). The regions affected by these storms are currently protected by an operational hail mitigation project. Differences with previously reported storms detected in the southern oasis are highlighted. Mendoza is a semiarid region situated roughly between 32S and 37S at the east of the highest Andes top. It forms a natural laboratory where different sources of gravity waves, mainly mountain waves, occur. In this work, we analyze the effects of flow over topography generating mountain waves and favoring deep convection. The joint occurrence of storms with hail production and mountain waves is determined from mesoscale numerical simulations, radar and radiosounding data. In particular, two case studies that properly represent diverse structures observed in the region are considered in detail. A continuous wavelet transform is applied to each variable and profile to detect the main oscillation modes present. Simulated temperature profiles are validated and compared with radiosounding data. Each first radar echo, time and location are determined. The necessary energy to lift a parcel to its level of free convection is tested from the Convective Available Potential Energy and Convection Inhibition. This last parameter is compared against the mountain waves' vertical kinetic energy. The time evolution and vertical structure of vertical velocity and equivalent potential temperature suggest in both cases that the detected mountain wave amplitudes are able to provide the necessary energy to lift the air parcel and trigger convection. A simple conceptual scheme linking the dynamical factors taking place before and during storm development is proposed.

Keywords: mountain waves, storms, Andes, Mendoza

1. Introduction

The magnitude of the energy transformations associated with the changes of phase of water in precipitating cumulus clouds, as well as the strong updrafts and downdrafts which often extend throughout much of the troposphere, explains that cumulus convection, especially deep, intense convection, can have an important effect on the dynamics and energetics of larger scale atmospheric systems. The cumulonimbus cloud or thunderstorm often produces large hail, severe wind gusts, tornadoes, and heavy rainfall. Many regions of the Earth depend almost totally upon cumulonimbus clouds for rainfall. Cumulonimbus clouds also play an important role in global energetics and in the general circulation of the atmosphere by efficiently transporting moisture and sensible and latent heat into the upper portions of the troposphere and lower stratosphere. They also affect the radiative budgets of the troposphere. Moreover, cumulonimbus clouds influence tropospheric air quality and the chemistry of precipitation (e.g. Cotton and Anthes, 1989).

Meteorological phenomena over complex terrain have generated interest among atmospheric scientists, who have explored them for decades. Terrain rugosity changes the atmospheric height at each location, giving place to different vertical tropospheric structures along a given region. When elements such as temperature or precipitation are considered, any mountain range shapes their local climate, leading to a pronounced feedback between orographic precipitation and the topographic relief (Roe et al., 2003). The temporal and spatial characteristics in mountain areas are inevitably determined by the total complex of these factors: latitude, continentality, altitude and topography operating together (Barry 2008).

Several decades ago, Sawyer (1956) found that the hills intensify precipitation over rain areas already determined by dynamical factors. Later, Lowndes (1968) suggested that the heaviest orographic precipitation occurs within warm sectors that are not characterized by large scale ascent. Smith (1979) had stated that one of the ways in which orography influences the weather is by controlling the rainfall distribution. With respect to this, Houze (2012) recently pointed out that orographic precipitation is not caused by topography but, rather, occurs when storms of a type that can take place anywhere (deep convection, fronts, tropical cyclones) form near or move over complex terrain. The effects of topography on air motion operate over a wide range of scales, from planetary-scale wave motion to micro-scale wave motion through

turbulence and mixing (Fritts and Alexander, 2003). Internal gravity waves (GWs) and in particular mountain waves (MWs) are one of the most important energy and momentum transport mechanisms throughout the atmosphere (e.g. de la Torre et al., 2012).

In the southern Hemisphere, there are extratropical regions that exhibit strong wave activity close to the Andes and to the Antarctic Peninsula (e.g., Eckermann and Preusse, 1999; de la Torre et al., 2012; Hierro et al., 2013 –hereinafter, HI13-). A considerable number of deep valleys mainly aligned from north to south are a scenario for the development of strong and frequent convection events between late spring and early autumn, sometimes followed by the production of hailstorms causing severe damage. If the convective instability and moisture flux convergence conditions are appropriate, convection may be triggered by the combination of factors such as upward motion over a frontal zone or diurnal warming and/or orographic lifting (Johns and Doswell, 1992). Moist air masses are then pumped from near the ground to their levels of free convection. As Doswell (2001) pointed out, it is possible to identify mesoscale processes other than those created by deep moist convection can be thought of in several groups: free "internal" instabilities, forced "external" processes, fronts, and GWs. In the case of GWs (Hooke, 1986), sometimes their amplitudes and size make them important for deep convection. This should take place at low levels, where potentially buoyant parcels exist (Eom, 1975). From observed deep convection events, Uccellini (1975), Stobie et al. [1983], Uccellini and Koch (1987) and Chimonas and Nappo (1987) pioneered the analysis of interactions between GWs and storms. Hooke (1986) pointed out the relevance of GWs amplitude during deep convection.

In the Cuyo region (Argentina), located east of the Andes Range at midlatitudes roughly between 30 and 37°S, high and middle frequency intrinsic GWs are permanently generated from different sources, in particular MWs. In this region, the presence of large amplitude MWs previous to deep convection events is frequent. Some storm developments are sometimes followed by intense hail production. Sánchez et al. (1999) stated that two ingredients are required for hail development: supercooled liquid water and a sufficient updraft. In USA, Koppel et al. (2000) observed that favorable conditions for the propagation of large-amplitude GWs during sufficient time to initiate deep convection are infrequent. In Spain, (Fraile et al., 2001) found that the maximum reflectivity (Z), the cell top height and the maximum Z height are considerably different between hail and no-hail storms.

The dynamics present in these events to the east of the Southern Andes Range was studied by several authors. de la Torre et al. (2004) found that an accumulation of moist enthalpy, sufficient instability conditions and the simultaneous presence of anabatic winds as the triggering mechanism generate deep convection. Other authors have noted in this region a maximum in low-level moisture roughly between 30-40S during the austral summer, associating this enhancement with deep convection (e.g. Velasco and Fritsch, 1987). In relation to this, Sánchez et al. (2008) considered 68 days with storm cells between 1984 and 2004. They found that 60% of these cases occurred during the austral summer, while 68 cases registered radar *Z* values higher than 55 dBz. García-Ortega et al. (2009) analyzed 128 storm days registered between 1994 and 2006 with *Z* over 45 dBz; in 118 cases, at least one storm cell showed *Z* values above 55 dBz. During storms with *Z* higher than 55 dbZ, the main effect is hail production, with significant negative effects on agriculture and hence on the local population. They concluded that convection was favored by the diurnal temperatures and regional topography, with the mountains and solar radiation playing key roles as activating mechanisms. Llamedo et al. (2009) analyzed two case studies and found two main modes of oscillation with horizontal wavelengths between roughly 50 and 200 km, clearly corresponding to MWs. MWs as a forcing of deep convection events over the study area were recently analyzed for case studies by de la Torre et al. (2011). From Convective Available Potential Energy (CAPE) and Convective Inhibition (CIN) results, they found that MWs could represent the main forcing for those cases.

Thirty-nine severe storm cases that occurred between 2006 and 2010 over a nearby region, situated to the south of that here considered were studied by HI13. Two samples of storms in the presence and absence of significant MWs were analyzed. The behavior of the precipitation flux, the maximum *Z* and the height top of the cell with maximum *Z* from the two samples were observed. Stationary modes with horizontal wavelengths between 40 and 160 km and a direction of propagation between −32° and 30° with respect to the zonal direction were identified. The vertical wavelength estimated for these structures is close to 7 km. Through the evaluation of several non-dimensional numbers relating storm and MWs energy, these authors found that MWs could provide enough energy to overcome the surface stable layer.

In the present manuscript, from radar and radiosonde data recorded between 2004 and 2011, some additional features to those previously described in HI13 regarding deep convection

events detected in the southern oasis, are now presented for the northern and central oasis. The possible relevance of the different terrain topographic structure in the triggering of deep convection events in the northern-central and southern oasis is first discussed. Next, we concentrate on a subset of 15 storms in the northern-central oasis registered in the presence of intense MWs. In Section 2, we describe the databases and simulations employed. The case studies selected and the methodology applied are described in Section 3. Section 4 describes the radar observations and some thermodynamic considerations and in Section 5, final considerations and a possible conceptual scenario are presented.

2. Radar data and mesoscale simulations

Cuyo is a semiarid region characterized by the presence of three cultivated oases (northern, central and southern) located along the Mendoza province. A three conventional weather radar network (two S- and one C-band) provides information about any storm generated and/or developed over the regions under study. These affected regions are currently protected by an operational hail prevention project conducted by the Government of Mendoza (www.contingencias.mendoza.gov.ar). This project includes the three radar network and an operational silver iodide seeding program by aircraft and ground generators. The radar data are integrated using the Thunderstorm Identification Tracking Analysis and Nowcasting (TITAN; Dixon and Wiener (1993)) radar software which provides composite images from the maximum *Z* values in overlapping areas The TITAN software defines a storm cell by an operational threshold of 35 dBz and 50 km^3 in volume within a spatial resolution of 1 km^3. (See HI13 for details). The vertical structure of the atmosphere is also observed from radiosounding (RS) data, provided by the Servicio Meteorólogico Nacional from Argentina (SMN - www.smn.gov.ar), corresponding to the Mendoza Aerostation located at 32.8S and 68.8W.

The mesoscale simulations were performed based on the Weather Research and Forecasting (WRF3.0) regional model (Skamarock et al., 2008) using the 1x1 NCEP (National Center of Environmental Prediction) Global Final Analysis (FNL) to construct initial and boundary conditions. The regional circulation, the vertical velocity (w) and temperature (T) fields were determined from these data. Three nested domains, with horizontal resolutions of 36 km (2500x2500 km extent), 12 km (1044x1080 km extent) and 4 km (456x564 km extent)

respectively were designed (Figure 1). Their vertical structure consisted in 43 levels and a spin-up of 24 h was considered for each case. The model setup used the same parameterization scheme as in de la Torre et al. (2011) and in (See HI13 for details). Figure 1 shows the three domains employed. The inner domain includes the orography (shaded) and the three cultivated regions (oases) in Mendoza. The northern and central oases respectively include the cities of Mendoza and Tunuyán (e.g., de la Torre et al., 2004).

3. Storms selected and MWs analysis

A radar data set of 120 storms in the northern-central oasis and 60 in the southern oasis reveal several differences in behavior and development, which justify a separate treatment. As an example, we first consider the total number of storm cells detected by TITAN reaching the altitude (=10 km) and Z (=55 dBZ) values able to produce hail. These are: 226 and 288 cells in central-northern and southern oasis respectively. In Figure 2a, the mean displacement direction of both sets as a function of time is different. By considering the first 2 hours and a half of development, a simple average displacement direction yields 79° and 65° for the northern-central and southern cells respectively, counting clockwise from north. Southern cells begin their development towards the east and then deviate northeastwards, probably due to physical parameters and updrafts with cyclonic vorticity that characterize these cells. The other region usually exhibits cells advected eastwards from their onset. The time required by every storm cell to reach hail threshold parameters in both regions is considerably different. From the unknown distribution and the considerable spread observed within each subset, a different treatment with a robust and resistant method seems advisable to observe its behavior. In Figure 2b, two boxplots represent this distribution of time data. The northern-central oasis shows a median of 18 min, sensibly less than the 39 min observed in the southern oasis. In the first case, the spread represented by the difference between upper and lower quartiles is almost half that observed in the southern oasis and is slightly skewed towards the longest times. This behavior may be related to a closer proximity to Precordillera and Cordillera in the northern oasis, thus giving rise to faster developments. This difference may be thought from another point of view: Robinson and Srivastava (1982) (see also references therein), from a numerical bidimensional model applied to the Fleming storm (in northern hemisphere), found that embryos starting on the (right) downshear edge of the updraft northern gave rise to hail of diameter greater than 1 cm. These in turn, may execute recirculations, with the number of

recirculations and the final hailstone size increasing with the proximity of the embryo starting position to the turnover location of the updraft. The horizontal sorting of particles in the sloping updraft gave rise to a bunching of particles that may manifest as a streaky hail pattern on the ground. Assuming homogeneous embryo distributions in both oasis, local background shear conditions may help to understand the difference between the duration of storm development at both regions.

For the present study, from the deep convection events database described above and detected in the northern-central region during the southern spring and summer (October to March), *T* and *w* simulations indicate that at least in 30 cases, considerable MWs were present in the absence of cold fronts. These results are similar to those obtained by HI13, who found MWs in almost 30% of the cases detected and analyzed over the southern oasis. Taking into account the small available number of RS data to validate our simulations, we reduced these 30 MWs cases to only 15. We recall that the largest amplitude MWs in the region are usually expected during wintertime, between June and August (e.g. de la Torre et al., 2012). As stated before, the Cuyo region is dominated by a north-south aligned orography. The synoptic, large scale circulation indicates that the prevailing winds over the overall region enter from the west, with slight daily variations. In general, the storm developments in the presence of MWs begin between 15UT and 22UT in 86% of the cases (UT=Local Solar Time+3). The lifetime of the storm cells is variable, from 1 to 4 h. From 5 hours before to the first radar echo signal (FRE) time, large amplitude MWs persist during each of the 15 events selected over the northern and central oases. Their *w* amplitudes close to the mountain tops are variable, with maximum peak to peak values within around 10 m/s (in particular, the 2 case studies described below). Detected events usually cause severe damage to agriculture, as registered by a 200 hailpads network regularly spaced every 5 km over this region (not shown). Following de la Torre et al (2011) and HI13, our aim is to explore, in the region considered, the influence of orography in the triggering of these storms, through MWs forcing and/or local vertical winds developed within the valleys during the diurnal cycle. A different set of deep convection events detected in the southern oasis have been already considered and discussed in HI13.

Following HI13, FRE is considered when the operational threshold is first exceeded (t = 0). A single FRE is restricted to a 20x20 km area. The presence of MWs is explored from simulated *w* fields above the mountain tops (600 hPa). The 15 storms set is listed in Table 1. It should be

noted that these events were chosen due to the intense MWs activity detected from WRF simulations. The wave activity, as it usually happens for hydrostatic and non-hydrostatic MWs, should be evident in every dynamic or thermodynamic parameter. Nevertheless, as in previous works [e.g., HI13], where high intrinsic period MWs are expected, we select our cases from *w* fields. From these simulations, we observe that a possible criterion to group the storms may be stated from two clearly different structures systematically observed among the storms and their positive and negative *w* signatures. One structure shows elongated bands aligned almost in north-south direction (Figure 3a). The second presents a bi-dimensional distribution and exhibits alternate fringes of much shorter, mostly in SW-NE direction (Figure 3b). From the 15 storm data set and within each group, we identify 2 and 13 events respectively. By observing the mean wind that forces the MWs, during the 1D structures an intense zonal gradient of zonal wind between 30 and 40S is present, veering to an increasing westerly mean wind with increasing latitude. In the 2D structures, at and below mountain tops levels, a prevailing intense negative meridional wind with almost no zonal contribution is observed. Figure 3a-b illustrates these 1- and 2D structures at 600 hPa, for the two cases study selected and discussed below, corresponding to the storms registered on 26 Feb 2006 and 17 Mar 2010, at FRE times, 21:13 and 20:40 UT respectively (hereinafter cases C1 and C2). These two cases studies were selected due to the unusually good agreement observed in *Z* fields between their simulations and their respective radar observations.

If the 2D *w* structures corresponding to every storm at their respective FRE times are averaged (Figure 3c), a similar MWs morphology to that observed for each individual case remains identifiable, reproducing a systematic positive and negative *w* signatures pattern bounded to the mountains. This means that the *w* field seems to be "frozen", independent of time, during several hours before each deep convection initiation. Additionally, "updraft" and "downdraft" mesoscale sectors above the terrain are defined. The last intense eastern fringe is usually positive. Additional non-stationary and considerably weaker *w* signatures, not shown in Figure 3, indicate a relative displacement with respect to the mountains (eastwards) with increasing local time during the afternoon. This weaker vertical wind is attributed to the diurnal cycle and the differential heating that generates local winds within or near to the valleys. Returning to the stationary MW structures, we now identify their main parameters. As is known, GWs display space-time perturbations that can be analyzed along horizontal, vertical or even slanted

directions (de la Torre et al., 2011). As stated before, *w* is an appropriate variable to detect and analyze non hydrostatic MWs (e.g. Smith, 1979). The structures are analyzed following our previous criterion in HI13. According to this criterion, we consider MWs over the considered region with prevailing horizontal wavelengths between 12 and 240 km. From simulated velocity components (*U, V, W*), the velocity perturbations components (*u'*, *v'*, *w'*) are obtained after removing the background flow (de la Torre et al., 2006). In doing so, we considered zonal profiles (ZP) at 600 hPa and latitudes 34.0 and 33.8S, coincident with FRE during C1 and C2. ZPs are regularly spaced within each inner (3rd) domain at 4 km. A high-pass non recursive filter with cutoff at 240 km was applied to *w'* (hereinafter, simply *w*). By subtracting filtered from not filtered ZPs, we then apply the filter once more to this difference, now with cutoff at 12 km. In doing so, we derive a band-pass filtered *w* ZP, including possible horizontal wavelengths (λ_H) between 12 and 240 km. Finally, we apply a Morlet continuous wavelet transform (CWT) (Torrence and Compo, 1998) to *w*, in order to determine the principal oscillation modes governing each case. Repeating the band pass procedure at different pressure levels and at the same latitudes as before, vertical wavelengths (λ_V) between 15 and 20 km, considerably longer than those detected in HI13, are evident (Figure 4a-b). By observing now ZPs at 600 hPa pressure level (roughly close to the mountain tops), two modes with λ_H = 30 and 100 km (C1) and with λ_H = 25 km (C2) are identified (Figure 4c-d respectively).

4. Thermodynamic aspects and radar observations

Following de la Torre et al. (2011) and HI13, the Convective Available Potential Energy (*CAPE)*, the convective inhibition (*CIN)* and the vertical kinetic wave energy per unit mass, k_E, are taken as representative magnitudes during the development of the storm energy. *CAPE* represents the energy available to lift air parcels (e.g., Emanuel, 1994). From its traditional definition, (e.g., Landel et al., 1999):

$$CAPE = \int_{LFC}^{NBL} g \frac{T_{V(par)} - T_{V(env)}}{T_{V(env)}} dz \quad (1)$$

here *g* and *z* are the acceleration of gravity and altitude, *LFC*, *NBL* and $T_{V(par,\ env)}$ are the level of free convection, the neutral buoyancy level and the virtual temperature of the selected parcel and environment, respectively. Following the last definition, *CIN* describes a stable surface

layer, which rising air parcels have to overcome to reach the unstable layer. In this last equation, *ILL* represents an initial lower level for the selected parcel. From its definition, and *CIN* <0:

$$CIN = \int_{ILL}^{LFC} g \frac{T_{V(par)} - T_{V(env)}}{T_{V(env)}} dz \quad (2)$$

Given the terrain irregularities in the region under study, we evaluate these quantities for air parcels which are lifted from boundary layer levels. In particular, we compare MWs k_E with the stable layer energy (given by *CIN*). Time evolution of these quantities is calculated for the levels with highest k_E, relating it with *CIN*. In Figure 5, these are shown for C1 and C2, at the latitudes corresponding to detected FRE positions. It may be observed that the diurnal variation of *CIN* shows constant very small values around zero during several hours before FRE, it is to say, between 15 and 21UT. The energy required to overcome *CIN* before FRE detection in both cases is less than an available $k_E \approx 10$ J/kg. The evolution of *CAPE* exhibits extreme variability. During C1, very low values before FRE time. During C2, it reaches 1200 J/kg at the early afternoon, finally decreasing to half this value before FRE. As in previous storm analyses (de la Torre et al., 2011, HI13), here we do not find consistent indications regarding a possible relevance of this parameter in the triggering and development of deep convection in the Mendoza region.

During C1, from *Z* imagery, one first cell above 45 dBz, situated at the southern end of the central oasis is detected at FRE (21:13UT) (Figure 6a). The development of this and subsequent growing cells covering also the northern oasis are observed advected to the east by dominant westerlies, with a clearly defined trajectory as stated above in relation to Figure 2. As shown in Figure 3a, an intense updraft region is observed immediately to the west of the FRE sector several hours before. The storms considered in Table 1, in particular in C1 and C2, are composed of many cells. Many of them are born within this updraft region, comprised between the northern and central oases and the Precordillera. In Figure 6b (23:58Z), the maximum storm development shows *Z* values above 60 dBz, leaving considerable hail precipitation and damage at ground level in the central oasis region. C2 exhibits similar features in the progressive development of multiple cells, starting from an initial FRE (20:43UT) above 45 dBZ over the southern half of the central oasis (Figure 6c and d). Several cells with

increasing *Z* grow simultaneously after 21:30UT. A maximum development is observed approaching midnight, at 00:58UT. A description of both storm tracks is represented in Figures 6e and 6f respectively, were composite of maximum reflectivity during the evolution of C1 and C2, between their early and final stages is shown.

As it is known (e.g., Bolton, 1980) the equivalent potential temperature (θ_E) is a possible measure in the mesoscale of the static stability in an unsaturated atmosphere. Under normal, stably stratified conditions, it increases with height. Inversely, if $\partial\theta_E/\partial z < 0$,, the atmosphere is unstable to vertical motions such as deep convection. θ_E may be defined by:

$$\theta_E = \theta_L exp\left[\left(\frac{3036}{T_L} - 1.78\right) r(1 + 0.448r)\right] \quad (3)$$

where

$$\theta_L = T\left(\frac{p_0}{p-e}\right)^{\kappa_d} \left(\frac{T}{T_L}\right)^{0.28r} \quad (4)$$

and

$$T_L = \frac{1}{\frac{1}{T_d - 56} + \frac{log_e\left(\frac{T}{T_d}\right)}{800}} + 56 \quad (5)$$

θ_L is the potential temperature (in K) at the lifting condensation level (LCL). T_L, T and T_d is the temperature of air at LCL, at pressure p and temperature of dew point at p, p_0 = 1000 hPa, e is the water vapor pressure, κ is the ratio of the specific gas constant to the specific heat of dry air at constant p and r is the mixing ratio of water vapor mass per mass [kg/kg]. Figure 7 shows the evolution of θ_E as a function of longitude and altitude at FRE latitude (2, 1 and 0 hours before FRE time) for C1 -7a to c respectively- and C2 -7d to f-. The development of increasing $\partial\theta_E/\partial z < 0$ at low levels before FRE time, simultaneous with the progressive accumulation of humidity, may be observed. These features are not evident at other latitudes in the same region during C1 and C2 respectively.

5. Summary and conceptual model

The mean displacement direction and the unknown distribution time required by storm cells to reach hail threshold radar parameters in both regions justify a separate treatment above the northern-central and southern oases. A possible reason for these differences may found in the geographic situation of the oases with respect to Precordillera and Cordillera. In the southern oasis, mountain tops do not exceed 4 km, while in the northern-central oasis they are well above 6 km. In addition, in the latter region the western limit of the oasis is situated 20-30 km from the mountains, while in the southern oasis this distance exceeds 200 km. From the 120 storms considered in the northern and central oases, 15 of them were selected for this study mainly because of their outstanding MWs amplitudes, without taking into account the fact that the most intense MWs are expected during wintertime. Two clearly differentiated structures are observed through the vertical wind simulations, such that each storm belongs to one of these types. Both structures appear to be frozen to the topography of the region, defining systematic updraft and downdraft sectors. GWs parameters are analyzed from band-pass and wavelet analysis, indicating in the two cases analyzed the presence of short (long) horizontal (vertical) wavelengths, as expected for high intrinsic period non-hydrostatic waves. Their amplitudes reach maximum peak-to-peak values close to 10 m/s at the latitudes corresponding to detected FRE positions. It may be observed that the diurnal *CIN* variation shows constant values equal to zero during several hours before FRE, that is to say, roughly between 15 and 21UT. The required intensity of k_E to overcome *CIN* occurs before FRE detection in both cases. In both cases, the time evolution and vertical structure of vertical velocity, the accumulation of lower level humidity and the vertical gradient of equivalent potential temperature suggest that the MW amplitudes, at first radar echo times and location, are able to provide the necessary energy to lift up the air parcel and trigger convection. We propose a simple conceptual scheme linking the dynamical factors taking place before and during storm development, which may be described for the two case studies as follows:

After an accumulation of specific humidity ($\partial q/\partial t > 0$) at lower levels, MWs are forced by the mean horizontal wind at and below 600 hPa, from either 1) N-NW (C1) or 2) W (C2). This gives rise to quasi bidimensional wave structures at leeside mainly above 700 hPa, with dominant horizontal wavelengths between 25 and 30 km, situated above the valleys, to the east of the Cordillera and Precordillera. These structures are always found at identical locations,

generating well defined and periodic positive and negative w sectors. The action of anabatic winds starting in the early afternoon generates additional updrafts above ground levels, but this contribution appears to be considerably less intense in relation to MW amplitudes (see, e.g., Figure 4a-b in de la Torre et al. (2004)). Summing up, 4 elements are taken into account: i) strong updraft-downdraft "bands" sectors (basically bi-dimensional) provided by MWs with w intensity typically greater than 3 m/s and located close to and above mountain top levels, ii) moderate updrafts (below 1m/s) starting in the afternoon at low levels due to the progressive heating of eastern mountain slopes (anabatic winds), iii) an accumulation of q and negative θ_E gradient at leeside low pressure levels and iv) a net circulation of humid air from sinks(sources) located below these downdraft (updrafts) assuming continuity and under compressibility conditions. We suggest that at the humidity accumulation locations and under appropriate unstable conditions, a pumping mechanism may provide the required uplift, to finally trigger deep convection. Following these arguments, during nighttime, katabatic valley winds (downward directed) may induce a negative contribution to the total updraft. This seems to be consistent with the considerably lower number of nighttime and early morning storms registered in the Cuyo region.

Acknowledgments: Manuscript prepared under grant CONICET PIP 11220090100649. A. de la Torre, R. Hierro, P. Llamedo and P. Alexander are members from CONICET.

References

Barry, R., 2008. Mountain weather and climate 3rd Edition. Cambridge, UK, Cambridge University Press.

Bolton, D., 1980. The Computation of Equivalent Potential Temperature. Mon. Wea. Rev., 108, 1046-1053.

Chimonas, G., Nappo, C.J., 1987. A thunderstorm bow wave. J. Atmos. Sci. 44, 533-541.

Cotton, W., Anthes, R., 1989. Storm and Cloud Dynamics. Academic Press, New York.

de la Torre, A., Daniel, V., Tailleux, R., Teitelbaum, H., 2004. A deep convection event above the Tunuyán Valley near to the Andes Mountains. Mon. Wea. Rev. 132, 2259-2268.

de la Torre, A., Alexander, P., Llamedo, P., Menéndez, C., Schmidt, T., Wickert, J., 2006. Gravity waves above the Andes detected from GPS radio occultation temperature profiles: jet mechanism? Geophys. Res. Lett. 33, L24810 http://dx.doi.org/10.1029/2006GL027343.

de la Torre, A., Hierro, R., Llamedo, P., Rolla, A., Alexander, P., 2011. Severe hail storms near southern Andes in the presence of mountain waves. Atmos. Res. 101 (1–2), 112–123, http://dx.doi.org/10.1016/j.atmosres.2011.01.015.

de la Torre, A., Alexander, P., Hierro, R., Llamedo, P., Rolla, A., Schmidt, T., Wickert, J., 2012. Large-amplitude gravity waves above the southern Andes, the Drake Passage, and the Antarctic Peninsula, J. Geophys. Res., 117, D02106, doi:10.1029/2011JD016377.

Dixon, M., Wiener, G., 1993. TITAN: thunderstorm identification, tracking, analysis and nowcasting, a radar-based methodology. J. Atmos. Oceanic Technol. 10, 785–797.

Doswell, C. A., 2001. Severe Convective Storms: An Overview. Meteorological Monographs, **28**, 1–26. doi: http://dx.doi.org/10.1175/0065-9401-28.50.1

Eckermann, S.D., Preusse, P., 1999. Global measurements of stratospheric mountain waves from space. Science, 286, 1534-1537.

Emanuel, K.A., 1994. Atmospheric Convection. Oxford University Press, New York .

Eom, J.K., 1975. Analysis of the internal gravity wave occurrence of 19 April 1970 in the Midwest. Mon. Weather Rev., 103, 217-226.

Fraile, R., Castro, A., Sánchez, J.L., Marcos, J.L., López, L., 2001. Noteworthy C-band radar parameters of storms on hail days in northwestern Spain. Atmos. Res. 59-60, 4161.

Fritts, D.C., Alexander, M. J., 2003. Gravity wave dynamics and effects in the middle atmosphere, Rev. Geophys., vol.41, doi:10.1029/2001RG000106.

García-Ortega, E., López, L., Sánchez, J.L., 2009. Diagnosis and sensitivity study of two severe storm events in the Southeastern Andes. Atmos. Res. 93, 161-178.

Hierro, R., Pessano, H., Llamedo, P., de la Torre, A., Alexander, P., Odiard, A., 2013. Orographic effects related to deep convection events over the Andes region Atmos. Res. 120, 216-225, http://dx.doi.org/10.1016/j.atmosres.2012.08.020.

Hierro, R., Llamedo, P., de laTorre, A., Alexander, P., Rolla, A., 2012. Climatological patterns over South America derived from GPS RO data. Journal of Geophysical Research, 117, D03116, doi:10.1029/2011JD016413.

Hooke, W.H., 1986. Gravity waves. Mesoscale Meteorology and Forecasting: In: Ray, P. (Ed.), Amer. Meteor. Soc., pp. 272-288.

Houze Jr., R.A., 2012. Orographic effects on precipitating clouds. Rev. Geophys. 50, RG1001.

Johns, R.H., Doswell, C.A., 1992. Severe local storms forecasting. Wea. Forecasting, **7**, 588-612.

Koppel, L.L., Bosart, L.F., Keyser, D., 2000. A 25-yr climatology of large amplitude hourly surface pressure changes over the conterminous United States. Mon. Wea. Rev. 128, 51-68.

Landel, G. J., Smith, A., Baeck, M.L., Steiner, M., Ogden, F.L., 1999. Radar studies of heavy convective rainfall in mountainous terrain, J. Geophys. Res., 104(D24), 3145131465, doi:10.1029/1999JD900297.

Llamedo, P., de la Torre, A., Alexander, P., Luna, D., Schmidt, T., Wickert, J., 2009. A gravity wave analysis near to the Andes Range from GPS radio occultation data and mesoscale numerical simulations: Two case studies. Adv. Space Res., 44, 494-500.

Lowndes, S., 1968. Forecasting large 24-h rainfall totals in the Dee and Clwyd River Authority Area from September to February. Meteor. Mag., 97, 226-235.

Robinson, W.D., and Srivastava, R.C., 1982. Calculations of hailstone growth in a sloping steady updraft. Atmosphere-Ocean, 20 (1), 76-89.

Roe, G.H., Montgomery, D.R., Hallet, B., 2003. Orographic precipitation and the relief of mountain ranges, J. Geophys. Res., 108, 2315, doi:10.1029/2001JB001521.

Sánchez, J.L., García, E., Marcos, J.L., Dessens, J., 1999. Formation of big and giant drops inside Mediterranean convective cells, Proc. EGS Plinius Conference held at Maratea, Italy, October 14-16, pages 57-65.

Sánchez, J.L., López, L., Bustos, C., Marcos, J.L., García-Ortega, E., 2008. Short term forecast of thunderstorms in Argentina. Atmos. Res. 88, 36-45.

Sawyer, J.S., 1956. The physical and dynamical problems of orographic rain. Weather, 11, 37581.

Skamarock, W.C., Klemp, J.B., Dudhia, J., Gill, D.O., Barker, D., Duda, M.G., Huang, X.-Y., Wang, W., 2008. A description of the advaced research WRF Version 3, NCAR Technical Note NCAR/TN-475+STR.

Smith, R.B., 1979. The inuence of mountains on the atmosphere. Adv. Geophys. 21, 87230.

Stobie, J.G., Einaudi, F., Uccellini, L.W., 1983. A case study of gravity waves convective storms interactions: 9 May 1979. J. Atmos. Sci. 40, 2804-2830.

Torrence, C., G.P. Compo, G.P., 1998. A practical guide to wavelet analysis. Bull. Am. Meteorol. Soc. 79, 61-78.

Uccellini, L.W., 1975. A case study of apparent gravity wave initiation of severe convective storms. Mon. Weather Rev. 103, 497-513.

Uccellini, L.W., Kock, S.E., 1987. The synoptic setting and possible energy sources for mesoscale wave disturbances. Mon. Weather Rev., 115,721-729.

Velasco, I., Fritsch, J.M., 1987. Mesoscale convective complexes in the Americas, J. Geophys. Res., 92(D8), 95919613, doi:10.1029/JD092iD08p09591.

Date	Structure
05 Jan 2005	2D
27 Dec 2005	2D
26 Feb 2006	1D
27 Nov 2008	2D
14 Jan 2009	2D
31 Dec 2009	2D
03 Jan 2010	1D
05 Jan 2010	1D
02 Feb 2010	2D
09 Feb 2010	2D
17 Mar 2010	2D
18 Nov 2010	2D
20 Nov 2010	2D
16 Feb 2011	2D
22 Feb 2011	2D

Table 1. Storm set selected in northern and central oasis. The simulated vertical wind (w) 1- or 2D structure is indicated (see text for explanation).

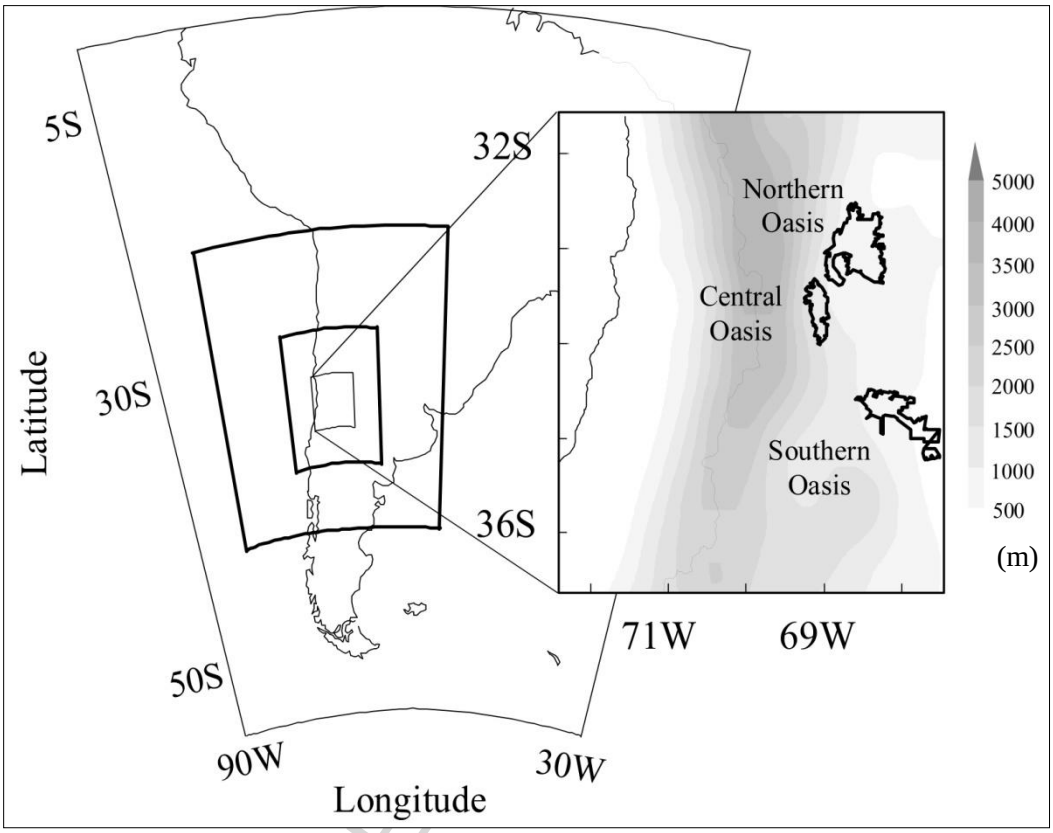

Figure 1. Three nested domains, with horizontal resolutions of 36 km (2500x2500 km extent), 12 km (1044x1080 km extent) and 4 km (456x564 km extent) respectively chosen for WRF simulations. The northern, central and southern oases are indicated.

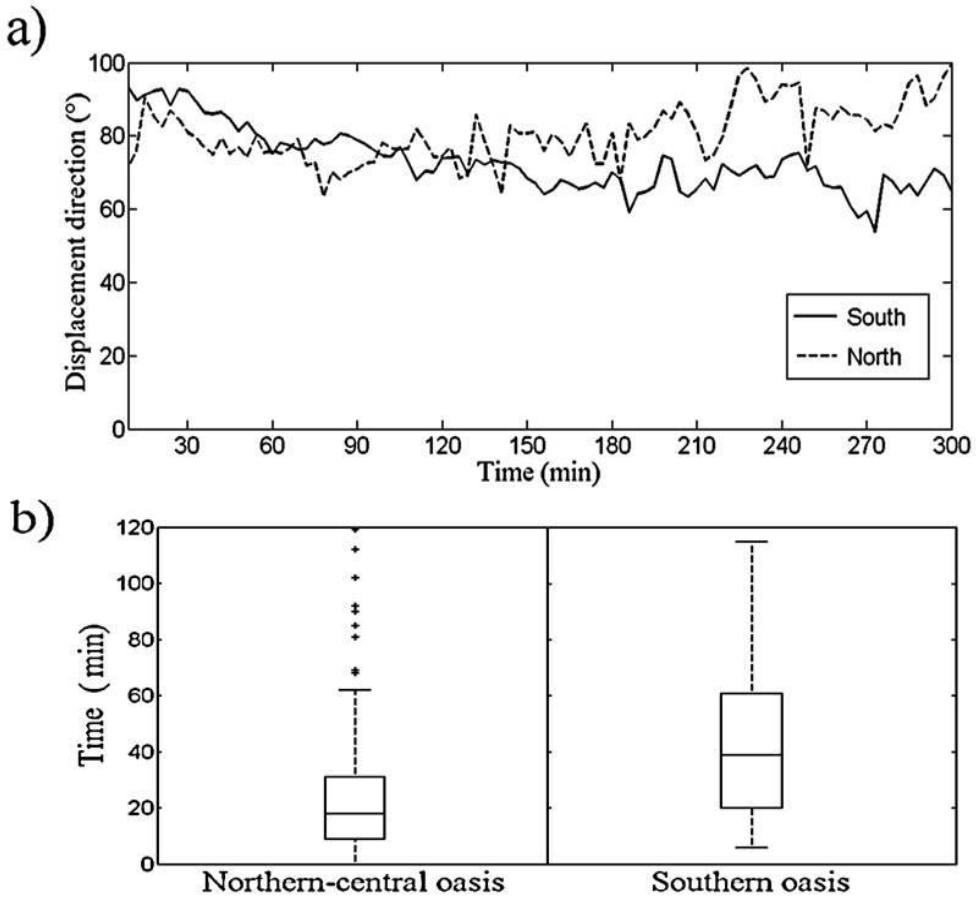

Figure 2. a) Mean displacement direction for northern-central and southern storm cells, from a set of 180 storms registered between 2004 and 2011 (see text). b) The time required by every storm cell to reach hail threshold parameters in both regions is considerably different. Two boxplots represent this distribution. The northern-central oasis shows a median of 18 min, sensibly less than the 39 min observed in the southern oasis. In the first case, the spread represented by the difference between upper and lower quartiles is almost half that observed in the southern oasis and is slightly skewed towards the longest times.

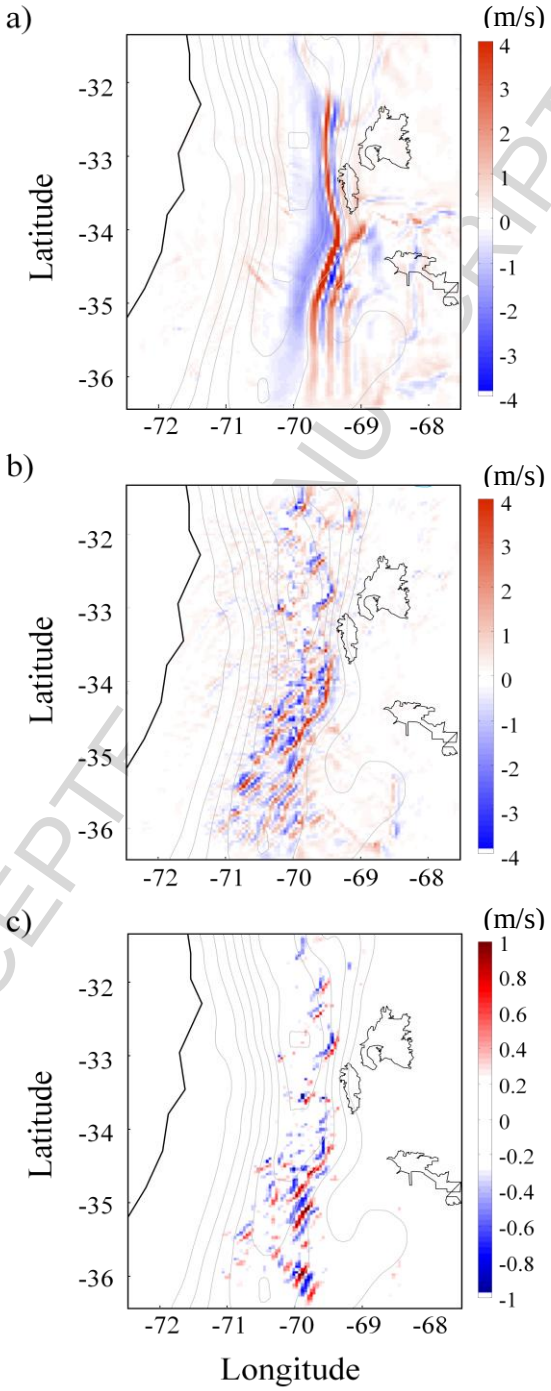

Figure 3. a) and b) *w* structures corresponding to the storms on 26 Feb 2006 and 17 Mar 2010, at FRE times 21:13 and 20:40 UT (cases C1 and C2 respectively). Isolines along and above the mountains represent constant altitude levels. c) Average of bidimensional *w* structures corresponding to 2D storm at their respective FRE times (see text). The *w* field seems to be "frozen" during several hours preceding each convection initiation.

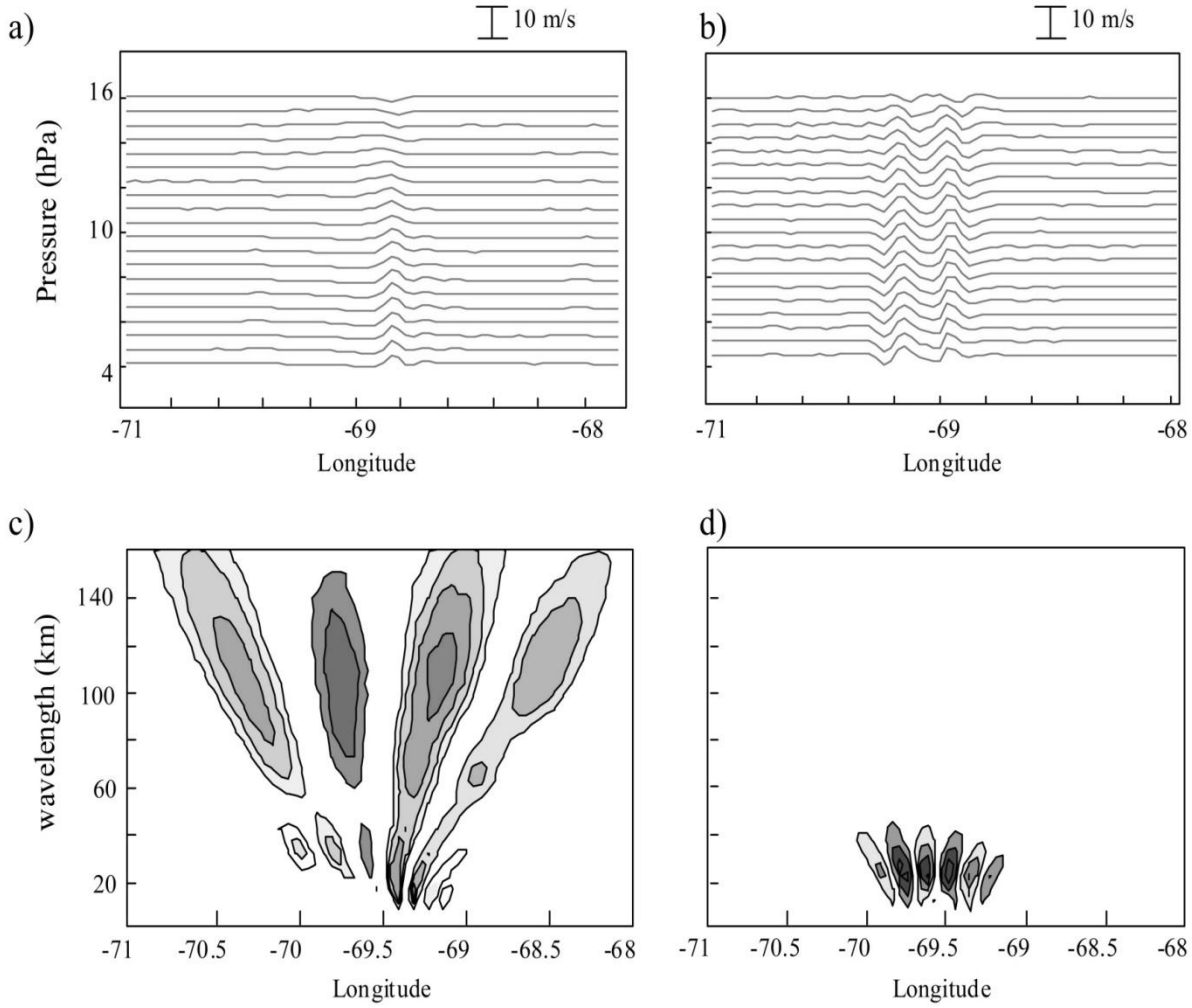

Figure 4. a)- b) Band-pass filtered *w* zonal profiles (ZPs) for decreasing pressure constant levels, at latitudes 34.0 and 33.8S, coincident with FRE during C1 and C2 respectively. c) - d) Morlet continuous wavelet transform from *w* ZPs at 600 hPa (roughly close to the mountain tops). Two modes with λ_H = 30 and 100 km (C1) and with λ_H = 25 km (C2) are identified.

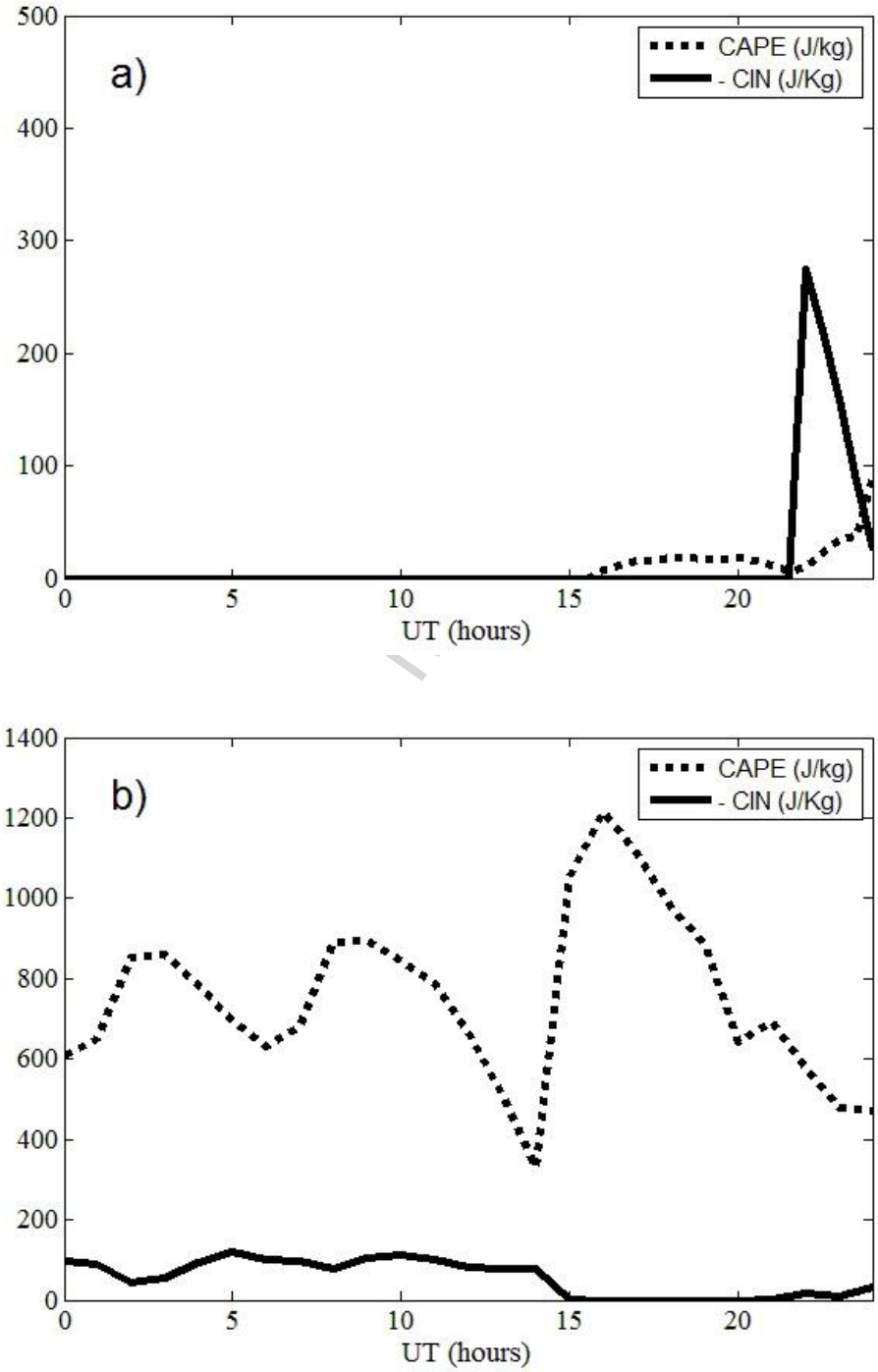

Figure 5. *CIN* and *CAPE* diurnal variability, for C1 (a) and C2 (b), at the latitudes corresponding to detected FRE positions.

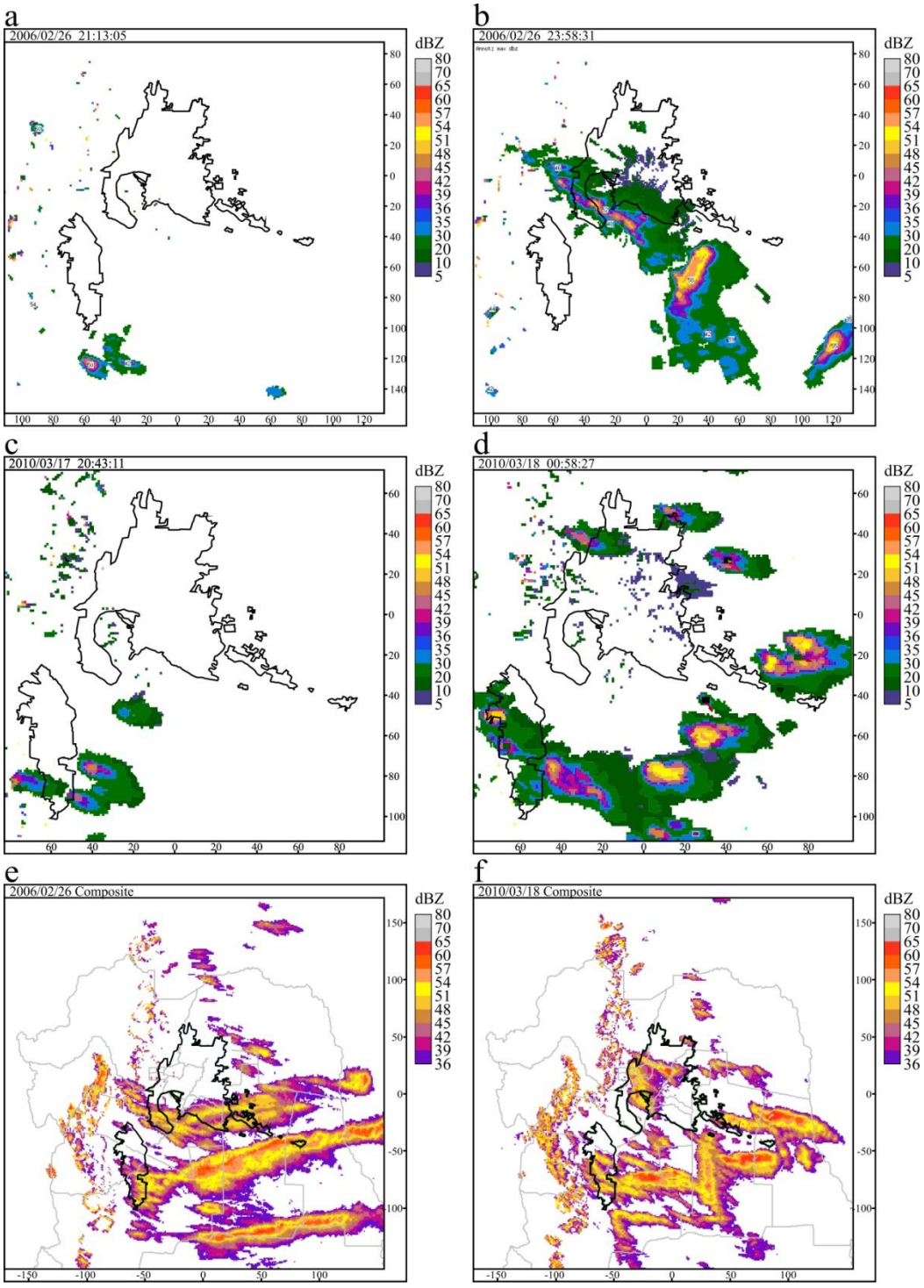

Figure 6. a) – b) First radar echo (FRE) and maximum storm development for C1. c) – d) The same, for C2. Composite of maximum reflectivity during the evolution of C1 (e) and C2 (f), between their early and final stages, respectively. A larger region including both oasis and the northern half of the province of Mendoza is here indicated.

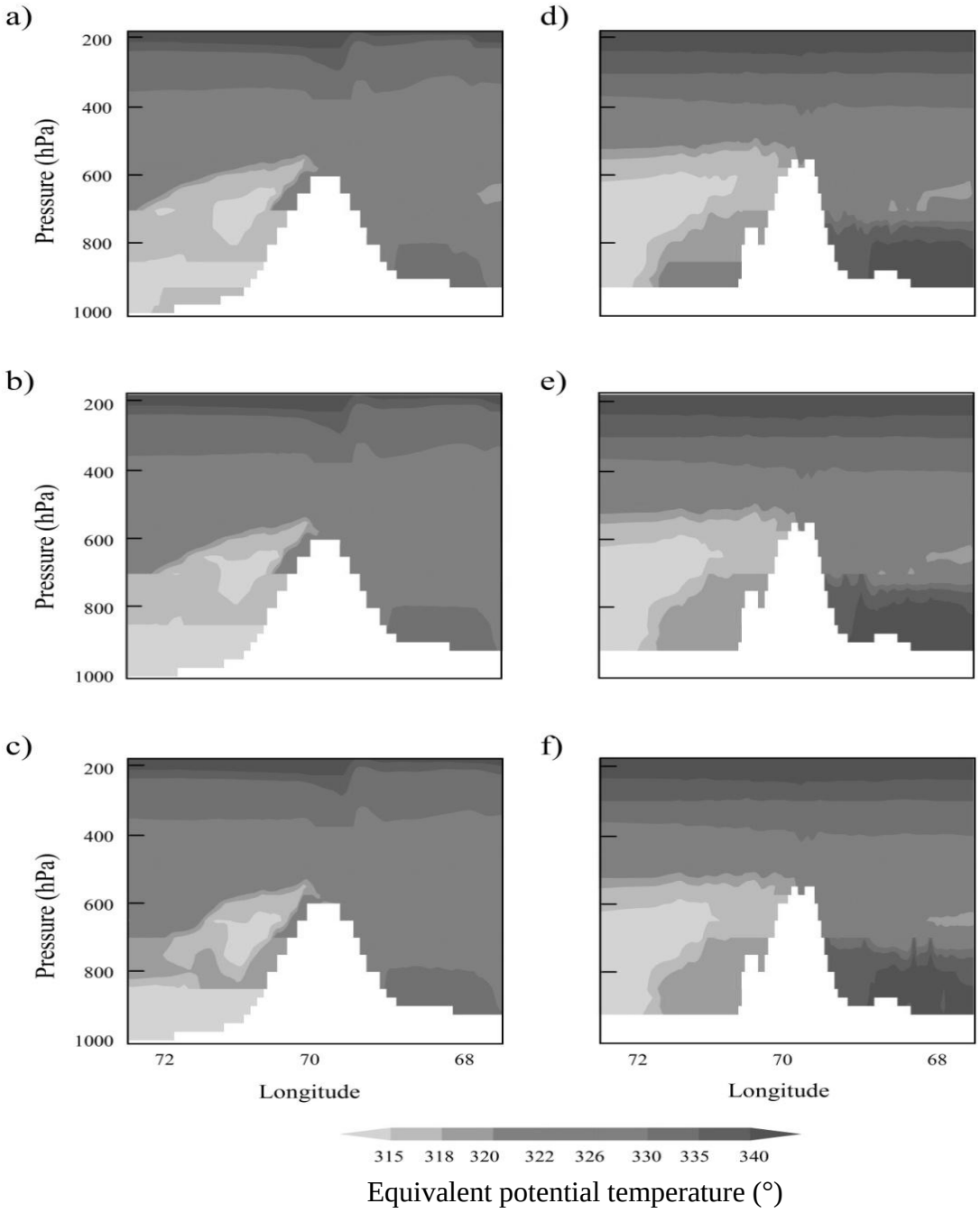

Figure 7. Time evolution of equivalent potential temperature (θ_E) as a tomographic longitude-altitude presentation, at FRE latitude at a) 2, b) 1 and c) 0 hours before FRE time (C1). d) to f) The same, for C2.

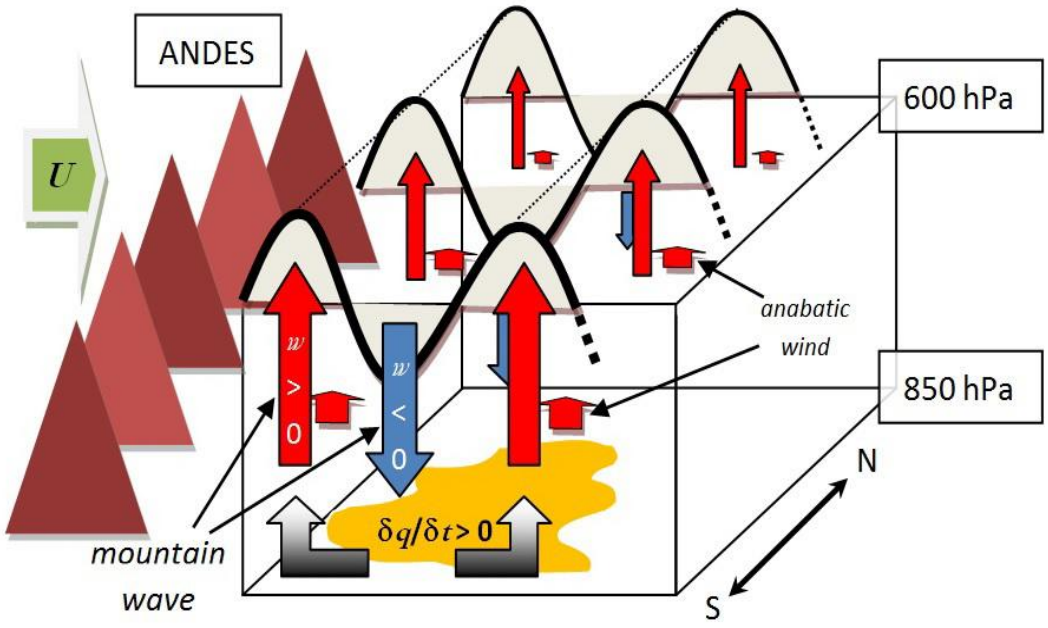

Figure 8. After an accumulation of specific humidity ($\partial q/\partial t > 0$) and a negative vertical gradient of equivalent potential temperature at lower levels, MWs are forced by the mean horizontal wind at and below 600 hPa, from either 1) N-NW (C1) or 2) W (C2). This gives rise to quasi bidimensional wave structures at leeside mainly above 700 hPa, with dominant horizontal wavelengths between 25 and 30 km, situated above the valleys, to the east of the Cordillera and Precordillera. These structures are always found at identical locations, generating well defined and periodic positive and negative w sectors. The action of anabatic winds starting in the early afternoon generates additional but much weaker updrafts above ground levels. Given continuity and incompressibility conditions, a pumping mechanism may provide the required uplift to trigger deep convection.

Highlights

Two structures of vertical air velocity are observed above the Mendoza Andes region ► In two case studies the mountain wave amplitudes are able to trigger convection ► A simple conceptual scheme linking the dynamical factors is proposed